Solid Freeform Fabrication 2024: Proceedings of the 35th Annual International Solid Freeform Fabrication Symposium – An Additive Manufacturing Conference
Reviewed Paper

Influence of novel space filling PBF-LB scanning strategies on part distortion and density

Maximilian Frey*, Max Frankenhauser*, Volker Schulze*, Frederik Zanger*

*wbk Institute of Production Science, Karlsruhe Institute of Technology (KIT),
Kaiserstr. 12, 76131 Karlsruhe, Germany

Abstract

Additive Manufacturing, especially Powder Bed Fusion – Laser Beam (PBF-LB), is known for its ability to create intricate designs with high precision. Yet, residual stresses remain a challenge, causing distortion. Novel laser paths, including various spiral and space-filling curves such as Hilbert, Gosper, and Peano, have been investigated. They were compared with standard stripe strategies. Parameters such as scan length and hatch distance are varied while maintaining energy density constant. Cantilever beams were used to measure distortion and density. Fractal strategies show minimal distortion with slight density loss. Spiral paths lead to a minimized porosity but show an increased distortion. Segmenting paths reduce distortion across all strategies. The orientation of the cantilever relative to the gas flow affects the distortion extent. Gosper and Hilbert curves reduce distortion with slight density reduction, while spiral paths minimize porosity but increase distortion. Segmenting paths effectively reduce distortion without density loss in all strategies.

1. Introduction

The Powder Bed Fusion – Laser Beam (PBF-LB) process has become a foundational additive manufacturing technology, enabling the production of highly complex and precise metal components. Despite its advantages, the PBF-LB process is often affected by residual stresses and distortion, which can significantly affect the dimensional accuracy and mechanical properties of the manufactured parts [1]. These issues are primarily attributed to the rapid heating and cooling cycles inherent to the PBF-LB process, which give rise to thermal gradients and, in turn, internal stresses [2]. These stresses can cause warping, detachment of the part from its support structure and cracks within the part [3].

The existing literature presents a variety of techniques for reducing residual stresses and distortion. One potential approach is to reduce temperature gradients by preheating the build plate. However, this strategy has the disadvantage of reducing energy efficiency, increasing the part-to-part time as well as the production costs [4–6]. Heat treatment performed after the build process can reduce the residual stresses generated during build-up [7]. However, this does not eliminate the possibility of stress-induced cracks occurring during the build process.

One of the most effective methods for the in-situ reduction of residual stresses is the implementation of optimized scanning strategies. Numerous exposure strategies have been developed to overcome the limitations of conventional strategies. The contour method, where the edge of each layer is exposed before filling the interior, has been shown to be effective in reducing distortion by better controlling the thermal profile [8]. Furthermore, strategies such as adaptive scanning, where the laser path is dynamically adjusted based on real-time thermal feedback, have

demonstrated the potential to minimize residual stresses and improve overall part quality but with limitations on newer production systems or experimental setups [9].

A frequently used scanning strategy is to arrange scan vectors stripe wise [10–13]. A bi-directional arrangement of the tracks has been shown to reduce part distortion [10]. It can be demonstrated that the majority of the residual stresses present in the welded structure are a consequence of the stresses along the welding paths [11]. Furthermore, these residual stresses increase in magnitude with an increase in the length of the scan vector. Scan vectors with a length of 5 mm have been identified as preferable for 316L [12]. Zaeh and Branner [14] have demonstrated that the arrangement of vectors in islands results in a notable reduction in distortion. An extension of the stripe strategy is the use of checkerboard patterns, in which islands positioned next to each other are twisted at a 90° angle to each other, but themselves consist of stripes [15]. In order to achieve homogenization of the residual stresses in the xy-direction and to prevent the formation of a preferred direction for stresses, each layer should be rotated, independent of the scanning strategy used [11,13].

The spiral helix scanning strategy was developed to reduce the deformation in the melted layer caused by large thermal gradients. Because the scan paths are different for each layer, the bonding strength is increased [16]. There are numerous ways in which one could expose the helix scanning strategy. For instance, the vectors could change direction after each exposure, or one could expose the vectors from the outside to the inside and vice versa [17]. The spiral helix strategy demonstrated a significantly change of distortion and porosity compared to a part manufactured using stripes [18].

Only a few publications address the use of fractal scanning strategies for PBF-LB. Sebastian et al. [19] demonstrated the fundamental suitability of fractal strategies in single weld track experiments. The use of Hilbert curves led to a weld pool with a homogeneous temperature distribution and a reduced temperature gradient compared to other scanning strategies [20]. The use of fractal strategies led to a significant reduction in distortion in PA12 [21]. Although plastic and metal are processed differently, it is anticipated that the trends between the two material classes can be transferred, given that warpage is primarily caused by temperature gradients and heat build-up. The temperature distribution, although different in magnitude, is considered transferable for both material classes.

Despite these advances, it remains a challenge to optimize exposure strategies to find a balance between build speed, dimensional accuracy, and porosity. This work proposes novel exposure strategies to further minimize distortion in the PBF-LB process. For this purpose, spiral and fractal patterns are used to expose the layers. First, samples were fabricated with the conventional stripe strategy. In a second step, cantilever beams with spiral and fractal scanning strategies were printed, and their distortion compared to the reference samples. Additionally, the densities of the novel scanning strategies were examined using microsections.

2. Materials and methods

Powder feedstock

The tests were conducted on 316L stainless steel supplied by m4p material solutions GmbH (Magdeburg, Germany) with a particle size distribution between 20-63 µm. The chemical composition of the powder used was determined by X-ray fluorescence (XRF) or optical emission spectrometry with inductively coupled plasma (ICP-OES) by the supplier, table 1.

The powder has been used for previous build jobs. Following each build job, the powder was subjected to sieving under argon using a 100 µm sieve. The powder is then sealed in airtight containers. Due to the constant equalization of the powder removed by components with virgin powder, it is not possible to determine the precise number of cycles the powder has undergone. However, the particle size was determined using dynamic image analysis on a camsizer X2 from Microtrac Retch GmbH (Haan, Germany). The powder shows usual distribution values of d_{10} = 27,74 µm, d_{50} = 38,59 µm, d_{90} = 54,17 µm.

Table 1: Chemical composition of the used 316L stainless steel powder particles in wt%.

Cr	Mn	Mo	Ni	Si	C	Fe
17.6	1.6	2.3	10.8	0.8	0.02	base

Measuring of distortion and density

Cantilever beams (figure 1) were used to examine the distortion of different scanning strategies. After the printing process was complete, the legs were cut 3 mm above the build plate using wire electrical discharge machining (EDM) to allow the residual stresses to relax and bend the upper part of the cantilever beam. The resulting distortion was quantified using an O-Inspect 3/2/2 coordinate measuring machine from Carl Zeiss IQS (Oberkochen, Germany) with a probing sphere diameter of 6 mm. The diameter was chosen to enhance the measured robustness due to the printed surface. In order to obtain an accurate representation of the entire surface deflection, the surface was scanned in a meandering pattern in a grid of 1 mm in length and 5 mm in width while maintaining a distance to the edges of 3 mm. This sensing method was selected because the distortion along the narrow cantilever side is negligible. In order to avoid damaging the measuring tip, the tip was lifted before moving to the next measuring point. The difference between the lowest and highest measuring points was idenitfied and used for the comparison of different scanning strategies. The lowest z-value is observed in the block, as the residual stresses in this area of the part are constrained due to the connection to the build plate. The highest deformation is found on the opposite edge. In some instances, some tortion of the cantilever beam is evident, but to such a minor degree that it can be disregarded.

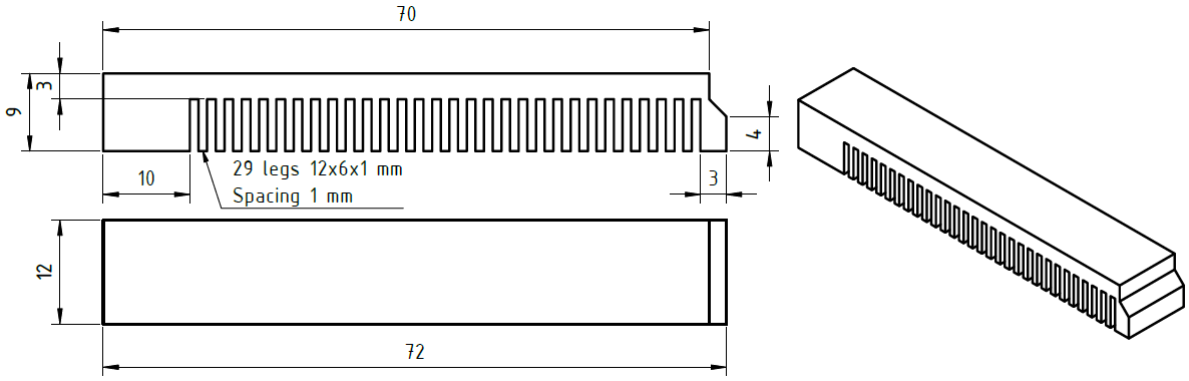

Figure 1: Technical drawing of cantilever beam used for evaluation of distortion [22].

To assess the density of the components, cubes with a length of 10 mm were printed. In order to determine the density, the surface was ground with a grain size of 2500 and then polished to 1 µm. The microsections were orientated in a way to enable visualization of the progression of porosity over the sample height. Two cubes were prepared per parameter set. An overview image with a magnification of x50 and three detailed measurements with a magnification of x300 per sample were taken using the VHX microscope from Keyence (Osaka, Japan). The density was evaluated using a grey value analysis in ImageJ.

Fabrication of test specimen

A SLM280HL machine from Nikon SLM Solutions AG (Lübeck, Germany) was used for the manufacturing of the specimen with a layer thickness of 50 µm and a preheating temperature of the build plate of 100 °C. The system is equipped with a 1070 nm ytterbium fiber laser from IPG Photonics (Marlborough, US). The laser beam is focused in the plane to d_0 = 82,3 µm with a varioscan system from Scanlab GmbH (Puchheim, Germany). The beam has a Rayleigh length of z_R = 3.62 mm. To avoid oxidation effects, the build chamber is flooded with argon. The oxygen content in the build chamber was controlled to remain below 200 ppm during the build job. A constant gas flow is used to remove spatter as well as welding fumes from the process zone. The used process parameters can be found in table 2. The volumetric energy density VED was held constant at 56 J/mm³. The following equation was used to calculate the VED:

$$VED = \frac{P}{v \cdot d \cdot h}$$

where P (W) is the laser power, v (mm/s) is the laser scanning speed, d (mm) is the hatch distance and h (mm) is the layer height.

Table 2: Process parameters used for the fabrication of the test samples.

	Laser power in W	Scanning speed in mm/s	Hatch distance in mm
Set A	235	700	0.12
Set B	308	917	0.12
Set C	380	1131	0.12

The positioning of the cantilevers on the build plate is illustrated in Figure 2. The xy-layout was employed to assess the impact of orientation relative to the gas flow, whereas the alternative configuration was utilized to reduce the number of required build jobs. For the configuration on the left, four pairs of cantilevers can be positioned on the build plate without compromising the

ability to cut the legs. In the configuration on the right, 16 different cantilevers can be positioned on the build plate.

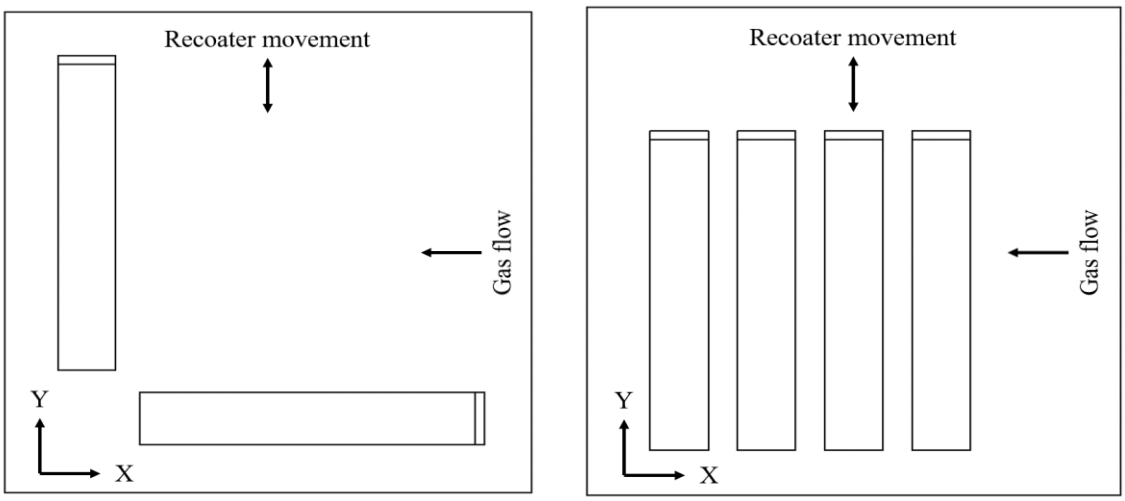

Figure 2: Positioning of cantilevers on the build plate. Left: xy-layout for evaluation of influence of distortion depending on the orientation relative to the gas flow, right: layout used to reduce number of build jobs needed.

The current generation of slicers is unable to process the recently developed scanning strategies. To address this issue, a bespoke workflow was created. The individual paths of each layer were created using AutoCAD from Autodesk (San Rafael, US) and the scan sequence to be performed later was defined simultaneously. The open-source software dxf2gcode was then used to convert the generated DXF file into g-code. In a final step, this code, which is optimized for milling, was converted into the CLI file format readable by the PBF-LB system using Python code. The speed specifications contained in the g-code were replaced by the scanning speed during the conversion.

Due to the geometry of the cantilevers and the necessity of manually drawing each layer, which cannot be achieved by a simple rotation, the dies of the cantilevers were created with the Magics slicer from Materialise (Leuven, Belgium). Standard stripes were utilized as the scanning strategy. Only the area above the feet, the actual bending beam, was exposed with the new scanning strategies. By using a uniform base with a defined initial state, the influence of the base on the resulting cantilever distortion can be neglected.

Scanning strategies

The scanning strategies that were investigated are shown in Figure 3. The stripe strategy was used for the reference cantilever beams. New scan patterns were used for the further investigations. In the spiral helix strategies, the hatch distance of 0.12 mm was kept constant (a) and increased continuously towards the center up to 0.18 mm or 0.24 mm (b) to avoid overheating in the center of the component. A variation of the square helix spiral is the hexagonal helix spiral (c). In all three cases, the exposure was from the outside to the inside. Furthermore, the three fractal strategies, namely Hilbert (d) [23], Peano (e) [24] and Gosper (f) [25], were examined.

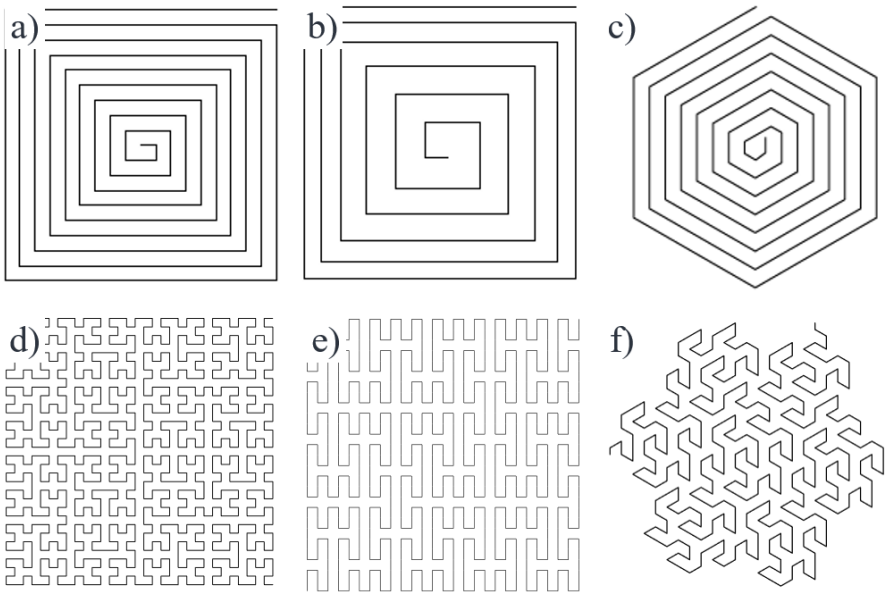

Figure 3: Examined scanning strategies: a) square spiral helix constant hatch, b) square spiral helix with divergent hatchdistance, c) hexagonal spiral helix constand hatch, d) Hilbert, e) Peano, f) Gosper.

In order to place the spirals on the cantilever, it is necessary to distribute several spirals next to each other on the surface. Due to the specified width of the cantilever, only integer multiples of this are possible as an island length. Island lengths of 4 and 6 mm were selected from the available options. Due to their shape, fractal strategies can be distributed more easily over the entire surface, without the necessity for grouping (see figure 4). Nevertheless, islands with an edge length of 4 mm were also created and exposed one after the other in order to investigate a possible influence. However, this change has no influence on the length of the scan vectors; only the exposure sequence can be altered.

Subsequent layers are rotated by 90° with respect to one another. According to [11,13], this should homogenize the residual stresses in the xy-plane. To prevent individual paths from lying on top of one another, the islands created in the spirals are also offset laterally so that the center point of the spiral from layer n coincides with the corner points of the spirals from layer n-1. In the fractal strategies, the layers were shifted 60 µm so that the paths lie in the gaps between the welding lines of the previous layers.

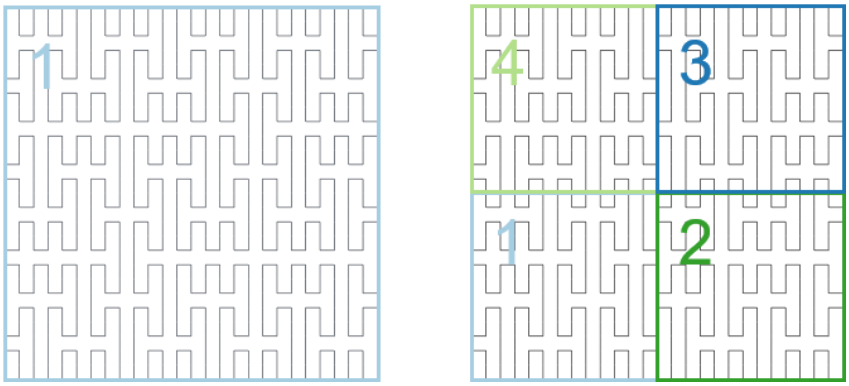

Figure 4: Island formation in fractal strategies using the example of the Peano curve
left: no islands on the part, right: scanning paths grouped in four islands for control of scan sequence

3. Results and Discussion

Influence of orientation relative to gas flow direction

The distortion of the cantilevers depending on their orientation to the gas flow direction is shown in figure 5. It can be observed that the distortion increases with the laser power, despite a nominally constant volume energy density. Furthermore, it can be seen that the orientation in the lower and middle range of the laser power has no significant influence on the distortion. However, at the higher laser power of 380 W, an orientation of the components perpendicular to the gas flow direction is preferable. One reason for the differences in distortion is the different cooling of the melt pool by the gas flow. This effect is not measurable with the two other laser energies investigated due to the lower melt pool temperatures. The assumption, which was not subjected to further investigation, is that the position on the build plate has a negligible effect on the distortion of the cantilever. Based on the findings, parameter set A (235 W) was selected for the fabrication of the cantilevers for subsequent investigations. The orientation of the cantilevers was chosen to be perpendicular to the direction of the gas flow to minimize the risk of damaging the recoater lip.

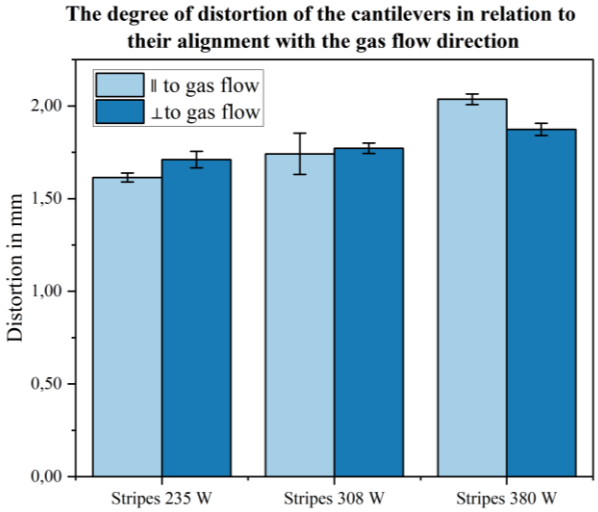

Figure 5: Distortion of cantilever beams orientated parallel and orthogonal to the gas flow direction.

Spiral strategies

Figure 6 shows the distortion of the spirals examined using the scanning strategies as well as the relative density. Depending on the orientation of the spirals and their arrangement in relation to each other, the distortion is more or less pronounced. It can be seen that the length of the scan vectors has no significant effect on the distortion in the area under consideration (figure 6, left). It can be assumed that the change between the two examined island sizes is not large enough. It can also be seen that a constant increase of the hatch distance towards the center can reduce the distortion if it is chosen appropriately. This can be explained by the reduced heat input and the ability of the heat introduced to flow away from the process zone, resulting in smaller temperature gradients. Hexagonal islands achieve the lowest distortion and are therefore preferable to square islands. A detailed analysis of the underlying mechanism is still pending.

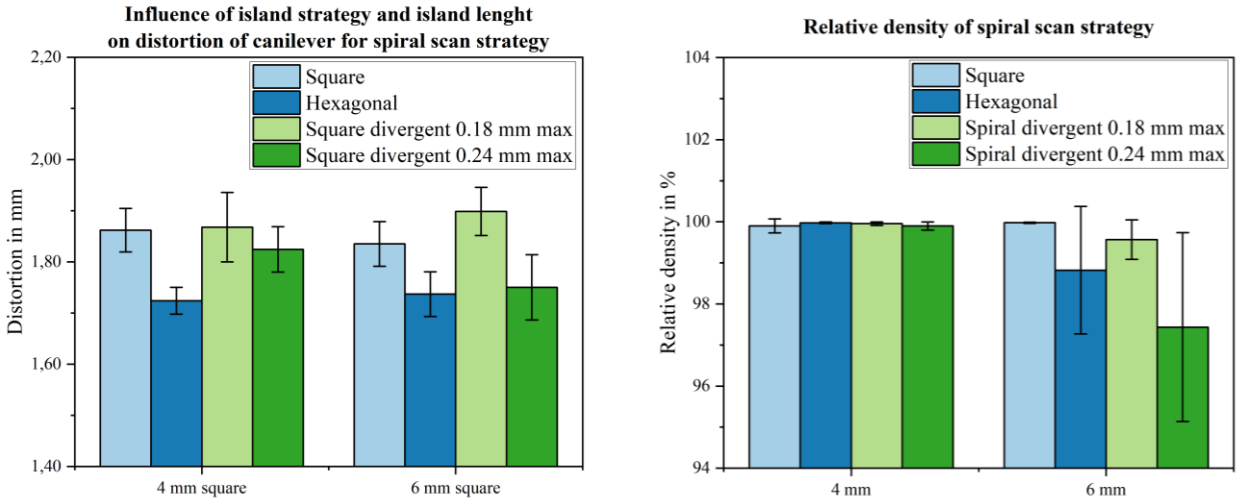

Figure 6: Spiral scanning strategies for different island strategies and lengths
left: distortion, right: relative density.

The density of 99.85 % is very high for all four variants examined when using 4 mm long islands. For the diverging spirals with a maximum spacing of 0.24 mm, there is a minimal decrease, but this cannot be considered significant due to the scatter. It remains to be investigated how far the maximum hatch distance can be increased. At an island length of 6 mm a strong scattering occurs especially for the hexagonal and diverging spirals with a maximum hatch distance of 0.24 mm, so that no clear statements can be made about the resulting component density. A possible reason for the scatter could be the choice of the density measurement used. Due to the microsections, only a portion of the porosity can be observed. The global porosity should be determined using Archimedes' principle, with the risk of open pores biasing the result. Figure 7 illustrates the prepared cross sections utilized for the determination of the relative density.

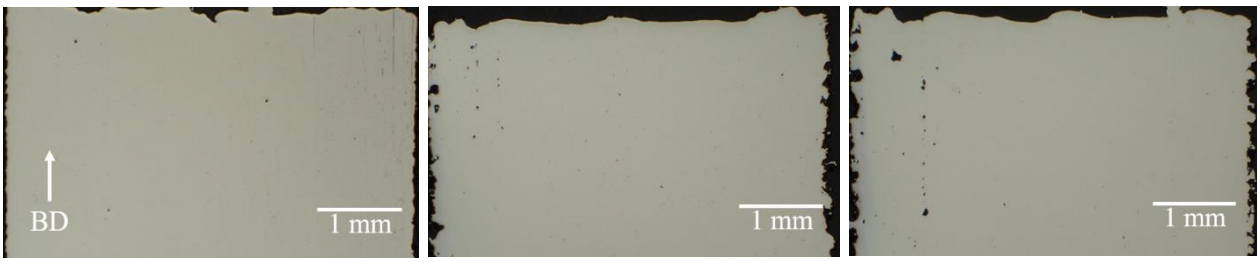

Figure 7: Microsections of spiral strategy with 4 mm square islands used for density determination. Left: constant hatch distance, middle: diverging hatch distance up to 0.18 mm, right: diverging hatch distance up to 0.24 mm.
BD = build direction.

Fractal strategies

A comparison of the three fractal strategies examined for their distortion behavior (Figure 8 left) shows that no significant change in distortion is identifiable, especially when no islands are used. This can be explained by the similarity of the structures. Due to the constant changes in direction of the laser paths within a layer, a very homogeneous stress distribution in the xy-plane can be expected. However, this was not determined in the experiments carried out. In comparison to the spirals, the distortion is somewhat lower, as the fractal strategies primarily involve short scan vectors up to 0.6 mm in length. When the strategies are arranged in islands, a strong scattering can

be observed in the cantilevers with Peano strategy, indicating an error in the construction job, particularly as the other two strategies exhibit a similar scattering without an island arrangement. Given that the fractal strategies are arranged in a manner that results in only a slight difference in exposure sequence compared to the full-surface variant, it is not apparent why the formation of islands in these strategies would have a significantly decisive effect on distortion.

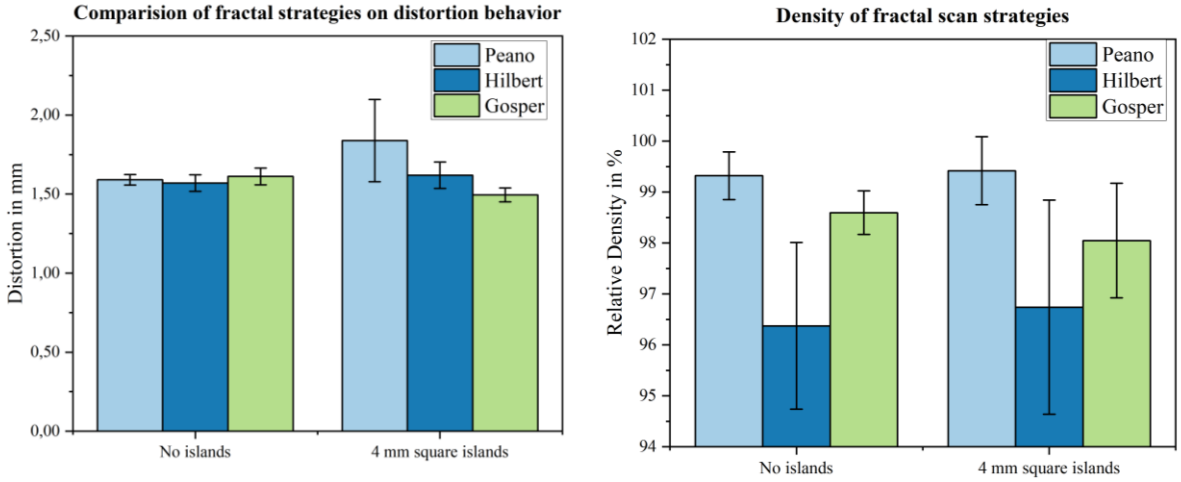

Figure 8: Distortion behavior (left) and relative density (right) of fractal scanning strategies.

A comparison of the density of the fractal strategies shows that the investigated Peano strategy has the best relative density of 99.35 % both when using a large area exposure and when forming islands. The Hilbert strategy has a much lower density of 96.70 %. A possible reason are the very short scan vectors used in this strategy which, as shown in literature, can increase the probability of pores. Due to laser beam turn-on delays and the time required to stabilize the melt pool after laser beam coupling, the desired melt path cannot be guaranteed. The measured density samples are presented in Figure 9. The presence of numerous lack of fusion pores provides empirical support for the thesis. A reduction in laser power below the desired level will also affect the distortion behavior of the cantilever an should be further investigated.

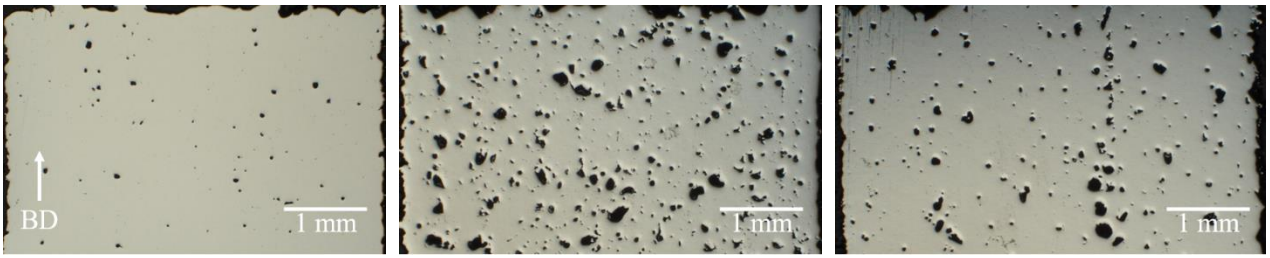

Figure 9: Microsections of fractal strategies without islands used for density determination.
Left: Peano, middle: Hilbert, right: Gosper.

Comparison of investigated scanning strategies

Figure 10 presents a summary of the results obtained in the examination. A comparison of the densities and maximum distortions achieved by the different scanning strategies reveals that the fractal strategies exhibit low distortion, yet also a relatively high porosity. In contrast, the spirals demonstrate high density, yet also high distortion. The greater distortion of the spirals in comparison to the strips is in direct contrast to the results of [18], which should be subjected to

further investigation. The stripe strategy is evident as the optimal approach, as it simultaneously achieves both high density and low distortion. Nevertheless, the Peano strategy also appears promising, exhibiting a slightly higher porosity content but even lower distortion. As the study was currently only carried out with a parameter set that was tested with the stripe strategy, there is hope that a further increase in density can be achieved with the fractal strategies, especially the Peano strategy, by adjusting the process parameters. The same argumentation can be applied to the spiral strategies.

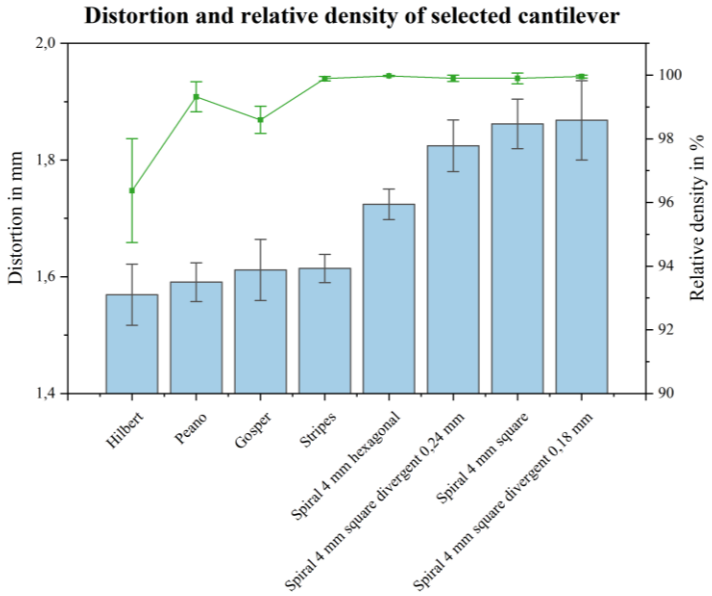

Figure 10: Comparison of the distortion behavior (blue bars) and relative density (green line) of various investigated scanning strategies.

4. Conclusion and Outlook

This study examined the impact of various scanning strategies on distortion behavior and resulting relative density. A CAD-file and a Python code were utilized to convert new scanning strategies into a code that could be read by the PBF-LB machine. The standard stripe strategie was employed as a reference and compared with spiral and fractal strategies. The distortion behavior of the various strategies was investigated in islands of varying lengths, with fractal strategies additionally examined over expansive areas. The findings can be summarized as follows:

- The degree of distortion increases with increasing laser power.
- The influence of part orientation relative to the gas flow is negligible for lower laser powers.
- The use of hexagonal islands for spiral helix strategies can reduce distortion while maintaining good relative density.
- To prevent overheating in the middle of the spiral, it is recommended that a diverging hatch distance be employed towards the middle.
- Fractal Strategies, especially Peano, have the potential to reduce the distortion behavior compared to the standard stripe strategy when density can be increased by adapting process parameters.

Further work should investigate the parameter adaptation to the new strategies in particular. The changed temperature balance offers significant opportunities to further increase the density of the components and to further reduce distortion. Additionally, only the distortion in the direction of build-up could be investigated in the present work. To utilize the strategies introduced in real components, it would be beneficial to determine the residual stresses in the respective spatial directions of the body. Given the geometry of the structures and the additional rotation of the layers in relation to each other, it is assumed that an almost homogeneous stress distribution can be found in the xy-direction.

5. Acknowledgements

The presented work was funded by the Ministry of Science, Research and the Arts of the Federal State of Baden-Wuerttemberg within the 'InnovationCampus Future Mobility', which is gratefully acknowledged.

References

[1] N.C. Levkulich, S.L. Semiatin, J.E. Gockel, J.R. Middendorf, A.T. DeWald, N.W. Klingbeil, The effect of process parameters on residual stress evolution and distortion in the laser powder bed fusion of Ti-6Al-4V, Additive Manufacturing 28 (2019) 475–484. https://doi.org/10.1016/j.addma.2019.05.015.

[2] P. Mercelis, J. Kruth, Residual stresses in selective laser sintering and selective laser melting, Rapid Prototyping Journal 12 (2006) 254–265. https://doi.org/10.1108/13552540610707013.

[3] N. Bastola, M.P. Jahan, N. Rangasamy, C.S. Rakurty, A Review of the Residual Stress Generation in Metal Additive Manufacturing: Analysis of Cause, Measurement, Effects, and Prevention, Micromachines 14 (2023) 1480. https://doi.org/10.3390/mi14071480.

[4] L. Papadakis, D. Chantzis, K. Salonitis, On the energy efficiency of pre-heating methods in SLM/SLS processes, Int J Adv Manuf Technol 95 (2018) 1325–1338. https://doi.org/10.1007/s00170-017-1287-9.

[5] S. Moritz, U. Ziesing, J. Boes, J. Lentz, S. Weber, M. Reuber, Influence of preheating temperatures on material properties of PBF-LB manufactured hot-work tool steel X37CrMoV5-1, Procedia CIRP 111 (2022) 171–175. https://doi.org/10.1016/j.procir.2022.08.143.

[6] P.D. Nezhadfar, A. Soltani-Tehrani, N. Shamsaei, Effect of Preheating Build Platform on Microstructure and Mechanical Properties of Additively Manufactured 316L Stainless Steel, (2019). https://doi.org/10.26153/TSW/17281.

[7] R. Barros, F.J.G. Silva, R.M. Gouveia, A. Saboori, G. Marchese, S. Biamino, A. Salmi, E. Atzeni, Laser Powder Bed Fusion of Inconel 718: Residual Stress Analysis Before and After Heat Treatment, Metals 9 (2019) 1290. https://doi.org/10.3390/met9121290.

[8] H. Ali, H. Ghadbeigi, K. Mumtaz, Effect of scanning strategies on residual stress and mechanical properties of Selective Laser Melted Ti6Al4V, Materials Science and Engineering: A 712 (2018) 175–187. https://doi.org/10.1016/j.msea.2017.11.103.

[9] J. Yang, H. Yu, J. Yin, M. Gao, Z. Wang, X. Zeng, Formation and control of martensite in Ti-6Al-4V alloy produced by selective laser melting, Materials & Design 108 (2016) 308–318. https://doi.org/10.1016/j.matdes.2016.06.117.

[10] C. Zhao, Y. Bai, Y. Zhang, X. Wang, J.M. Xue, H. Wang, Influence of scanning strategy and building direction on microstructure and corrosion behaviour of selective laser melted 316L

stainless steel, Materials & Design 209 (2021) 109999. https://doi.org/10.1016/j.matdes.2021.109999.
[11] L. Parry, I.A. Ashcroft, R.D. Wildman, Understanding the effect of laser scan strategy on residual stress in selective laser melting through thermo-mechanical simulation, Additive Manufacturing 12 (2016) 1–15. https://doi.org/10.1016/j.addma.2016.05.014.
[12] J.A. Kanko, P. Sibley, A. Boulger, The effect of scan pattern on the mechanical properties of laser powder bed fusion additive manufactured 316L stainless steel, in: Proceedings of the 27th Annual International Solid Freeform Fabrication Symposium, 2016: pp. 870–884.
[13] Z. Zheng, B. Sun, L. Mao, Effect of Scanning Strategy on the Manufacturing Quality and Performance of Printed 316L Stainless Steel Using SLM Process, Materials 17 (2024) 1189. https://doi.org/10.3390/ma17051189.
[14] M.F. Zaeh, G. Branner, Investigations on residual stresses and deformations in selective laser melting, Prod. Eng. Res. Devel. 4 (2010) 35–45. https://doi.org/10.1007/s11740-009-0192-y.
[15] Y. Lu, S. Wu, Y. Gan, T. Huang, C. Yang, L. Junjie, J. Lin, Study on the microstructure, mechanical property and residual stress of SLM Inconel-718 alloy manufactured by differing island scanning strategy, Optics & Laser Technology 75 (2015) 197–206. https://doi.org/10.1016/j.optlastec.2015.07.009.
[16] Q. Bo, S. Yu-sheng, W. Qing-song, W. Hai-bo, The helix scan strategy applied to the selective laser melting, Int J Adv Manuf Technol 63 (2012) 631–640. https://doi.org/10.1007/s00170-12-3922-9.
[17] A.H. Nickel, D.M. Barnett, F.B. Prinz, Thermal stresses and deposition patterns in layered manufacturing, Materials Science and Engineering: A 317 (2001) 59–64. https://doi.org/10.1016/S0921-5093(01)01179-0.
[18] D. Hagedorn-Hansen, M. Bezuidenhout, D. Dimitrov, T. Oosthuizen, THE EFFECTS OF SELECTIVE LASER MELTING SCAN STRATEGIES ON DEVIATION OF HYBRID PARTS, SAJIE 28 (2017). https://doi.org/10.7166/28-3-1862.
[19] R. Sebastian, S. Catchpole-Smith, M. Simonelli, A. Rushworth, H. Chen, A. Clare, 'Unit cell' type scan strategies for powder bed fusion: The Hilbert fractal, Additive Manufacturing 36 (2020) 101588. https://doi.org/10.1016/j.addma.2020.101588.
[20] S.S. Babu, L. Love, R. Dehoff, W. Peter, T.R. Watkins, S. Pannala, Additive manufacturing of materials: Opportunities and challenges, MRS Bull. 40 (2015) 1154–1161. https://doi.org/10.1557/mrs.2015.234.
[21] S. Schlicht, S. Greiner, D. Drummer, Low Temperature Powder Bed Fusion of Polymers by Means of Fractal Quasi-Simultaneous Exposure Strategies, Polymers (Basel) 14 (2022) 1428. https://doi.org/10.3390/polym14071428.
[22] Hexagon, Simufact Additive, (2021).
[23] D. Hilbert, Ueber die stetige Abbildung einer Line auf ein Flächenstück, Math. Ann. 38 (1891) 459–460. https://doi.org/10.1007/BF01199431.
[24] G. Peano, Sur une courbe, qui remplit toute une aire plane, Math. Ann. 36 (1890) 157–160. https://doi.org/10.1007/BF01199438.
[25] J.W. Cannon, B.B. Mandelbrot, The Fractal Geometry of Nature., The American Mathematical Monthly 91 (1984) 594. https://doi.org/10.2307/2323761.